

Dualities and Topological Classification of the $S = 1$ Pyrochlore Spin Ice

Sena Watanabe* and Yukitoshi Motome†

Department of Applied Physics, The University of Tokyo, Tokyo 113-8656, Japan

Haruki Watanabe‡

*Department of Physics, The Hong Kong University of Science and Technology, Clear Water Bay, Hong Kong, China
Institute for Advanced Study, The Hong Kong University of Science and Technology, Clear Water Bay, Hong Kong, China and*

Department of Applied Physics, The University of Tokyo, Tokyo 113-8656, Japan

(Dated: March 5, 2026)

We resolve the phase diagram of the $S = 1$ pyrochlore spin ice, which exhibits trivial paramagnetic, U(1) Coulomb, and spin nematic phases. In the monopole-free limit, the system can be effectively mapped onto 3D XY and Ising loop-gas models depending on the spin anisotropy, which provides theoretical estimates for the phase boundaries, while a macroscopic flux vector classifies the topological sectors via geometric parity rules. At finite temperatures, thermal monopoles act as a symmetry-breaking field in the continuous XY wave picture and topologically sever defect strings in the loop-gas picture, rounding the phase transitions into continuous crossovers. These theoretical findings are corroborated by classical Monte Carlo simulations.

Introduction.— The quest to understand highly frustrated magnets has driven the discovery of exotic states of matter that defy conventional symmetry-breaking paradigms [1–4]. A quintessential example is the classical Ising (or effective spin-1/2) spin ice on the pyrochlore lattice [5–11]. In these systems, strong local geometrical frustration forces the spins to obey the celebrated “two-in, two-out” ice rules. This local constraint allows the microscopic spin degrees of freedom to be coarse-grained into an emergent, divergence-free effective magnetic flux field $\nabla \cdot \mathbf{B} = 0$, where $\mathbf{B} = \nabla \times \mathbf{A}$. In the low-temperature limit, where magnetic monopoles—defective tetrahedra violating the ice rules—are suppressed, the macroscopic physics is captured by an emergent U(1) gauge theory governed by the effective Maxwell action [9, 12, 13], $S_{\text{eff}}[\mathbf{A}] = \frac{\kappa}{2} \int d^3r (\nabla \times \mathbf{A})^2$.

This emergent electromagnetism dictates an unconventional state of matter: while devoid of conventional long-range magnetic order, the system exhibits an infinite correlation length with an algebraic decay of spin correlations. The transverse nature of the gauge field leads to characteristic dipolar correlations [11], which manifest as distinctive “pinch points” in momentum space [10, 14, 15]. This highly entangled, fluctuation-dominated regime is known as the Coulomb phase. At any finite temperature, however, thermally excited magnetic monopoles [16, 17] act as a mobile magnetic plasma. This plasma induces Debye screening [18, 19], which exponentially cuts off the long-range dipolar correlations and degrades the Coulomb phase into a conventional paramagnet.

While the spin-1/2 spin ice is well understood, releasing the rigid spin-length constraint opens a frontier for emergent phenomena, including magnetic moment fragmentation [20, 21], fractionalized spin liquids [22], and exotic spin nematics [23, 24]. Very recently, Pandey and Damle investigated a spin-1 extension of the pyrochlore

antiferromagnetic Ising model [25], building on related developments in bipartite dimer-loop models [26, 27]. In this model, the spins can additionally occupy a nonmagnetic $S^z = 0$ state, whose relative statistical weight is controlled by a fugacity parameter w determined by the single-ion anisotropy. Through large-scale Monte Carlo (MC) simulations, they unveiled a phase diagram characterized by three distinct regimes: a trivial paramagnetic phase for $w < w_{c_1}$, a \mathbb{Z}_2 deconfined Coulomb phase [i.e., a full U(1) Coulomb phase] for $w_{c_1} < w < w_{c_2}$, and a \mathbb{Z}_2 confined Coulomb phase (a spin nematic state) for $w > w_{c_2}$. Based on finite-size scaling analyses, Pandey and Damle suggested that the transitions at w_{c_1} and w_{c_2} belong to the 3D XY and 3D Ising universality classes, respectively [25]. The nature of such topological phases and confinement transitions has long been a central theme in condensed matter physics and lattice gauge theories [28–31], with implications extending even to water ice [32], hydrogen-bonded ferroelectrics [33], and phononic band insulators [34]. However, a unified theoretical framework capable of clarifying the microscopic origins of these universality classes—and their ultimate fate at finite temperatures—has been lacking.

In this Letter, we provide a theoretical description of this phase diagram by developing a dual formulation rooted in the principles of statistical mechanics [35]. Specifically, we establish mappings of the $S = 1$ model onto standard statistical mechanics models defined on the dual diamond lattice. In the small- w regime, the system maps onto a classical 3D XY model, demonstrating that the transition at w_{c_1} belongs to the 3D XY universality class. In the large- w regime, the geometric proliferation of $S^z = 0$ defects is described by a closed loop-gas representation that is isomorphic to the high-temperature expansion of the classical 3D Ising model, establishing the 3D Ising nature of the transition at w_{c_2} . Furthermore, we treat finite-temperature effects, showing that the ther-

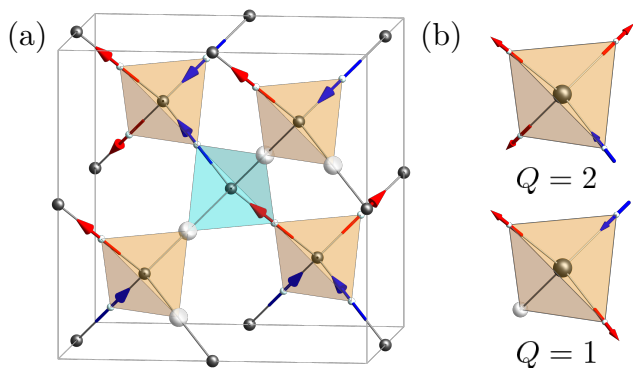


FIG. 1. (a) Geometric correspondence between the diamond and pyrochlore lattices. Black spheres represent the diamond sites, which are located at the centers of the cyan and orange tetrahedra formed by the pyrochlore sites. Arrows on the pyrochlore sites denote the spin-1 variables aligned with the local z -axis. Red and blue arrows represent $S_\ell^z = 1$ and $S_\ell^z = -1$, respectively, while white spheres correspond to $S_\ell^z = 0$. The illustrated spin configuration satisfies the ice rule. (b) Monopole charges and their corresponding spin configurations. Odd monopole charges can exist in the spin-1 model.

mal excitation of monopoles explicitly breaks the emergent continuous symmetry in the small- w regime and acts as a topological severing of defect strings in the large- w regime, thereby rounding the phase transitions into continuous crossovers.

Model.— We consider a classical spin-1 model of the Blume-Capel type [36, 37] on the pyrochlore lattice. Its sites reside at the midpoints of the nearest-neighbor links $\ell = \langle \mathbf{r}_A, \mathbf{r}_B \rangle$ of the underlying bipartite diamond lattice. The local positive z -axis for each spin $S_\ell^z \in \{-1, 0, 1\}$ points from \mathbf{r}_A to \mathbf{r}_B . This geometry is illustrated in Fig. 1. The system consists of L^3 cubic unit cells, each of linear size 1, subject to periodic boundary conditions. Each unit cell contains 8 diamond-lattice sites and 16 pyrochlore sites, totaling $N := 8L^3$ diamond-lattice sites and $2N$ spins.

The Hamiltonian $H := J \sum_{\langle \ell, \ell' \rangle} S_\ell^z S_{\ell'}^z + \Delta \sum_{\ell} (S_\ell^z)^2$, comprising a nearest-neighbor exchange J and a singleton anisotropy $\Delta := J + \mu$, can be recast into a perfect-square form:

$$H = \frac{J}{2} \sum_{\mathbf{r}} Q_{\mathbf{r}}^2 + \mu \sum_{\ell} (S_\ell^z)^2, \quad (1)$$

where the local monopole charge $Q_{\mathbf{r}} := \nabla \cdot \mathbf{S}_{\mathbf{r}}$ is the discrete divergence of the spin configuration at any diamond-lattice site \mathbf{r} (belonging to either sublattice A or B), defined as

$$\nabla \cdot \mathbf{S}_{\mathbf{r}_A} := \sum_{\ell \in \mathbf{r}_A} S_\ell^z, \quad \nabla \cdot \mathbf{S}_{\mathbf{r}_B} := - \sum_{\ell \in \mathbf{r}_B} S_\ell^z. \quad (2)$$

Introducing the fugacities $w := e^{-\mu/T}$ and $v := e^{-J/(2T)}$,

the partition function $Z := \sum_{\{S_\ell^z\}} e^{-H/T}$ is rewritten as

$$Z = \sum_{\{Q_{\mathbf{r}}\}} \sum_{\{S_\ell^z\}} \left(\prod_{\mathbf{r}} \delta_{\nabla \cdot \mathbf{S}_{\mathbf{r}}, Q_{\mathbf{r}}} \right) v^{\sum_{\mathbf{r}} Q_{\mathbf{r}}^2} w^{\sum_{\ell} (S_\ell^z)^2}. \quad (3)$$

For $J \gg T$ ($v \ll 1$), thermal monopoles are suppressed, and states satisfying the ice rule $Q_{\mathbf{r}} = 0$ dominate.

Duality Mapping to the XY Model.— To describe the small- w regime, we perform a duality transformation in the monopole-free limit ($v = 0$), building on the well-known mapping of divergence-free current models onto the XY model [38, 39]. Gauss's law constraint $\nabla \cdot \mathbf{S}_{\mathbf{r}} = 0$ is enforced by introducing a continuous phase field $\theta_{\mathbf{r}} \in [0, 2\pi)$ via the Fourier integral $\delta_{\nabla \cdot \mathbf{S}_{\mathbf{r}}, 0} = \int_0^{2\pi} \frac{d\theta_{\mathbf{r}}}{2\pi} e^{-i\theta_{\mathbf{r}} \nabla \cdot \mathbf{S}_{\mathbf{r}}}$. By inserting this into the partition function and performing a discrete integration by parts on the lattice, $\sum_{\mathbf{r}} \theta_{\mathbf{r}} \nabla \cdot \mathbf{S}_{\mathbf{r}} = - \sum_{\ell = \langle \mathbf{r}_A, \mathbf{r}_B \rangle} (\theta_{\mathbf{r}_B} - \theta_{\mathbf{r}_A}) S_\ell^z$, we find that the partition function factorizes over links:

$$Z_{v=0} = \int \mathcal{D}\theta \prod_{\langle \mathbf{r}, \mathbf{r}' \rangle} [1 + 2w \cos(\theta_{\mathbf{r}} - \theta_{\mathbf{r}'})], \quad (4)$$

where $\mathcal{D}\theta := \prod_{\mathbf{r}} \frac{d\theta_{\mathbf{r}}}{2\pi}$. For sufficiently small w , the Taylor expansion $\ln(1 + X) \approx X$ holds, yielding

$$Z_{v=0} \approx \int \mathcal{D}\theta e^{2w \sum_{\langle \mathbf{r}, \mathbf{r}' \rangle} \cos(\theta_{\mathbf{r}} - \theta_{\mathbf{r}'})}. \quad (5)$$

This is the partition function of the classical 3D XY model defined on the diamond lattice. The emergent XY spins interact with an effective ferromagnetic coupling $K = 2w$. Because the higher-order harmonics neglected in the Taylor expansion correspond to irrelevant operators in the renormalization-group sense, this mapping guarantees that the continuous phase transition at w_{c_1} belongs to the 3D XY universality class, providing a theoretical foundation for the recent numerical conjecture [25]. Using the numerical estimate for the critical coupling $K_c \approx 0.7877$ [40], we estimate the critical fugacity for the U(1) Coulomb phase onset to be $w_{c_1} = K_c/2 \approx 0.3939$. The deviation from the numerical result $w_{c_1} = 0.3609(1)$ obtained by Pandey and Damle [25] may stem from the higher-order terms in the generalized XY action.

Mapping to the Loop-Gas Model.— The approximation used for the dual XY mapping breaks down in the large- w regime. We therefore introduce a real-space “loop-gas” picture, a conceptual framework useful for understanding extended defects and confinement transitions [41, 42]. For the system of N diamond-lattice sites and $2N$ links, the links at $v = 0$ are predominantly occupied by $S_\ell^z = \pm 1$ spins due to their large weight, while $S_\ell^z = 0$ states (relative weight $1/w$) act as minority defects. The ice rule dictates that these defect strings never possess endpoints and must form closed-loop configura-

tions C . Thus, the partition function is given by

$$Z_{v=0} = w^{2N} W(\emptyset) \sum_C \frac{W(C)}{W(\emptyset)} \left(\frac{1}{w}\right)^{|C|}, \quad (6)$$

where $W(C)$ is the number of valid background spin configurations for a fixed closed-loop configuration C .

We evaluate this ratio using Pauling's approximation. Assuming that all $2N$ links can freely take $S_\ell^z = \pm 1$, the number of loop-free vacuum configurations is $W(\emptyset) \approx 2^{2N} (3/8)^N$, where $3/8$ is the probability of satisfying the ice rule at each of the N sites. For a configuration C consisting of $|C|$ links in total, these links are fixed to $S_\ell^z = 0$, leaving $2N - |C|$ free links. Furthermore, assuming no loop intersections, the configuration C traverses exactly $|C|$ sites. Thus, the system contains $N - |C|$ loop-free sites and $|C|$ loop-traversed sites. At the loop-free sites, the probability of satisfying the ice rule remains $3/8$. Conversely, at the loop-traversed sites, two of the four connecting links are fixed to zero, increasing the probability that the remaining two free links sum to zero to $\binom{2}{1}/2^2 = 1/2$. Thus, the number of valid configurations compatible with C is $W(C) \approx 2^{2N-|C|} (3/8)^{N-|C|} (1/2)^{|C|}$. Taking the ratio to the vacuum weight yields the configurational entropy reduction factor $W(C)/W(\emptyset) \approx 2^{-|C|} (3/8)^{-|C|} (1/2)^{|C|} = (2/3)^{|C|}$. This gives

$$Z_{v=0} \approx w^{2N} W(\emptyset) \sum_C \left(\frac{2}{3w}\right)^{|C|}. \quad (7)$$

This loop gas is isomorphic to the high-temperature expansion of the zero-field 3D Ising model. In terms of Ising spins $\sigma_r \in \{-1, 1\}$, the partition function $Z_{\text{Ising}} = \sum_{\{\sigma_r\}} \exp\left(K \sum_{\langle r, r' \rangle} \sigma_r \sigma_{r'}\right)$ can be expanded as

$$Z_{\text{Ising}} = (\cosh K)^{2N} 2^N \sum_C x^{|C|}, \quad (8)$$

where $x := \tanh K$. The proliferation transition of the loop gas, marking the onset of the U(1) Coulomb phase, maps onto the ferromagnetic transition of this Ising model [43]. While the bare weight $x \approx 2/(3w)$ relies on Pauling's approximation, which neglects short-range spatial correlations such as loop self-intersections, these geometric corrections correspond to irrelevant local perturbations that merely renormalize the effective fugacity without altering the universality class. This isomorphism establishes that the topological confinement transition at w_{c_2} falls into the 3D Ising universality class, explaining the critical exponents observed numerically [25]. Consequently, equating the theoretical estimate with the critical point $K_c \approx 0.3698$ [44] via $\frac{2}{3w_{c_2}} \approx \tanh K_c$, we predict $w_{c_2} \approx 1.884$. The agreement with the numerical result 1.8904(1) [25] demonstrates that this mapping captures the essential physics, with the deviation reflecting the higher-order corrections to Pauling's approximation.

Topological Classification via Global Flux.— At $v = 0$, the macroscopic global flux threading the system,

$$\mathbf{P} := \frac{1}{L} \sum_{\ell=\langle \mathbf{r}_A, \mathbf{r}_B \rangle} (\mathbf{r}_B - \mathbf{r}_A) S_\ell^z, \quad (9)$$

acts as a topological invariant that distinguishes the three phases. Since the vertical displacement along any link is $|z_B - z_A| = 1/4$, the system can be partitioned by $4L$ horizontal planes. Let C_k be the set of links intersecting the k -th plane. The net flux $W_z^{(k)}$ crossing this plane is given by

$$W_z^{(k)} = \sum_{\ell \in C_k} \text{sgn}(z_B - z_A) S_\ell^z. \quad (10)$$

The ice rule ensures that this flux is conserved across any plane ($W_z^{(k)} = W_z$), yielding $P_z = W_z \in \mathbb{Z}$. By cubic symmetry, $\mathbf{P} \in \mathbb{Z}^3$.

The parity of P_z can be evaluated modulo 2. The total number of links crossing a plane is $4L^2$. Since $S_\ell^z \equiv (S_\ell^z)^2 \pmod{2}$ and the geometric sign satisfies $\text{sgn}(z_B - z_A) \equiv 1 \pmod{2}$, we find $P_z \equiv \sum_{\ell \in C_k} (S_\ell^z)^2 \pmod{2}$. If we let n_0 be the number of $S_\ell^z = 0$ defect links intersecting the plane, the sum counts the number of nonzero links; thus, the remaining $4L^2 - n_0$ links must have $(S_\ell^z)^2 = 1$. Since $4L^2$ is an even integer, we obtain the congruence relation:

$$P_z \equiv 4L^2 - n_0 \equiv n_0 \pmod{2}. \quad (11)$$

Thus, the parity of the global flux is tied to the parity of n_0 . This geometric property dictates the macroscopic topological sectors. In the trivial phase ($w < w_{c_1}$), directed $S_\ell^z = \pm 1$ closed loops are dilute and cannot wrap around the periodic boundaries, freezing the macroscopic flux to $\mathbf{P} = \mathbf{0}$. In the U(1) Coulomb phase ($w_{c_1} < w < w_{c_2}$), both directed $S_\ell^z = \pm 1$ loops and undirected $S_\ell^z = 0$ strings proliferate. The macroscopic $S_\ell^z = 0$ strings can cross a plane an odd number of times [$n_0 \equiv 1 \pmod{2}$], unlocking the parity constraint and permitting all integer flux sectors ($\mathbf{P} \in \mathbb{Z}^3$). Finally, in the spin nematic phase ($w > w_{c_2}$), the $S_\ell^z = 0$ strings cease to proliferate. Finite closed loops must traverse a plane an even number of times, enforcing $n_0 \equiv 0 \pmod{2}$. This parity constraint eliminates odd flux sectors [$\mathbf{P} \in (2\mathbb{Z})^3$], encapsulating the \mathbb{Z}_2 flux-confined Coulomb phase where macroscopic $S^z = 0$ strings are confined and only the $S^z = \pm 1$ loops proliferate. This parity-based topological classification parallels the exact description of the 3D toric code limit using macroscopic loop parities [45]. As is evident, this topological nature relies on the absence of monopoles ($v = 0$). Once finite-temperature effects are introduced, these topological distinctions become blurred.

Finite-Temperature Effects.— At any finite temperature $T > 0$, the monopole fugacity v is small but finite.

By incorporating the leading effect of $0 < v \ll 1$ and repeating the XY mapping in the small- w regime, we find that the partition function becomes [46]

$$Z \approx \int \mathcal{D}\theta \exp \left(2w \sum_{\langle \mathbf{r}, \mathbf{r}' \rangle} \cos(\theta_{\mathbf{r}} - \theta_{\mathbf{r}'}) + 2v \sum_{\mathbf{r}} \cos \theta_{\mathbf{r}} \right). \quad (12)$$

Physically, thermal monopoles introduce a sine-Gordon term acting as a uniform external magnetic field. This field explicitly breaks the continuous $U(1)$ symmetry of the dual XY model, rounding the phase transition into a continuous crossover.

An analogous conclusion emerges in the large- w loop-gas representation. Incorporating thermal monopoles allows strings to possess endpoints. The loop-gas partition function is generalized to a sum over general graphs G ,

$$Z \approx w^{2N} W(\theta) \sum_G \left(\frac{2}{3w} \right)^{|G|} (\sqrt{3}v)^{|\partial G|}, \quad (13)$$

where $|G|$ is the number of links in the graph, and $|\partial G|$ denotes the total number of endpoints. This matches the high-temperature expansion of the 3D Ising model in a uniform magnetic field h , defined as

$$Z_{\text{Ising}} = \sum_{\{\sigma_{\mathbf{r}}\}} \exp \left(K \sum_{\langle \mathbf{r}, \mathbf{r}' \rangle} \sigma_{\mathbf{r}} \sigma_{\mathbf{r}'} + h \sum_{\mathbf{r}} \sigma_{\mathbf{r}} \right). \quad (14)$$

As detailed in the Supplemental Material [46], this yields

$$Z_{\text{Ising}} = (\cosh K)^{2N} (\cosh h)^N 2^N \sum_G x^{|G|} y^{|\partial G|}, \quad (15)$$

with the effective parameters identified as $x := 2/(3w)$ and $y := \sqrt{3}v$. Since a uniform magnetic field eliminates the phase transition in the effective Ising model, the macroscopic topological singularity of the proliferation transition in the original model degrades into a continuous crossover due to the topological severing of strings at $v > 0$. We note that an analogous explicit breaking of emergent gauge symmetries by relevant perturbations has been shown to impact confinement transitions in hydrogen-bonded systems [33]. This topological fragility contrasts sharply with 3D \mathbb{Z}_2 topological phases, such as the 3D toric code [45, 47] and exactly solvable Kitaev spin liquids [48, 49], where strict local constraints ensure the absence of string endpoints. In those models, the macroscopic loop parity (or Wilson loop) remains a robust topological order parameter, thereby preserving sharp finite-temperature phase transitions [45, 49].

Monte Carlo Simulations.— To verify our theoretical predictions, we perform classical MC simulations of the original microscopic spin model. We fix $J = 1$ throughout the following discussion. A standard MC sweep consists of $2N$ single-spin heat-bath updates, corresponding

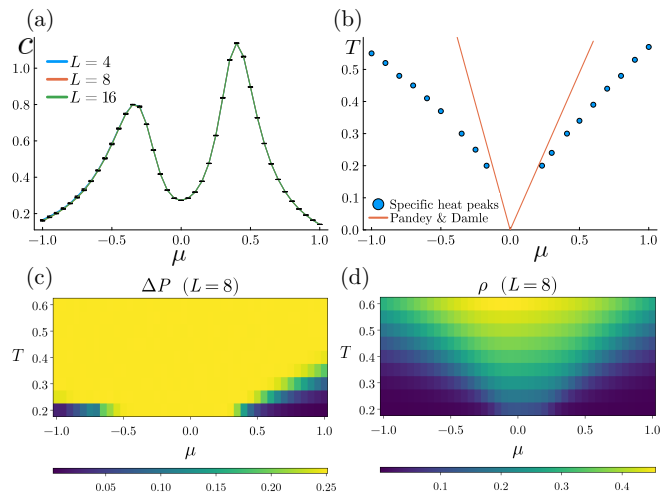


FIG. 2. Results of MC simulations. (a) System-size dependence of the specific heat at $T = 0.3$. (b) Peak positions of the specific heat for $L = 4$ and the phase boundaries determined numerically in the monopole-free limit by Pandey and Damle [25]. Heat maps of (c) the deviation ΔP and (d) the monopole density ρ for $L = 8$. Panels (c) and (d) indicate that the presence of thermal monopoles causes the macroscopic flux to deviate from integer values.

to the total number of spins in the system. For typical parameters, thermalization is performed for 10^6 sweeps starting from a random initial state, followed by 5×10^6 sweeps for measurements. In the highly frustrated regime (small Δ), we employ a hybrid scheme combining the short-loop algorithm [50, 51] with standard heat-bath updates to accelerate relaxation. For these runs, thermalization is performed for 10^5 sweeps, followed by 5×10^5 measurement sweeps. We calculate the specific heat per diamond-lattice site,

$$c = -\frac{T}{N} \frac{\partial^2 F}{\partial T^2} = \frac{1}{N} \frac{\langle E^2 \rangle - \langle E \rangle^2}{T^2}, \quad (16)$$

where E is the total energy. We also compute the macroscopic global flux \mathbf{P} and the monopole density,

$$\rho = \frac{1}{N} \left\langle \sum_{\mathbf{r}} |Q_{\mathbf{r}}| \right\rangle. \quad (17)$$

In the presence of monopoles, the flux \mathbf{P} is not restricted to \mathbb{Z}^3 or $(2\mathbb{Z})^3$. We define ΔP to measure the deviations of \mathbf{P} from integer values:

$$\Delta P = \sum_{i=x,y,z} \left\langle (P_i - [P_i])^2 \right\rangle, \quad (18)$$

where $[\cdot]$ denotes the nearest integer.

As the parameters are tuned across the predicted boundaries, the specific heat exhibits broad maxima. MC data for three different system sizes in Fig. 2(a) reveal that the peak height of c saturates and does not

grow with increasing linear system size L . This absence of a macroscopic thermodynamic divergence provides numerical evidence that, at finite temperatures ($v > 0$), the phase transitions are rounded into continuous crossovers due to the explicit symmetry breaking by thermal monopoles. The peak positions of the specific heat are plotted in Fig. 2(b). We observe that the peak positions deviate from the phase boundaries in the monopole-free limit reported by Pandey and Damle [25] as the temperature T increases (i.e., as v becomes larger). This behavior supports the conclusion that the phase transitions are smeared into crossovers.

Furthermore, the measurements of \mathbf{P} visualize the loss of topological quantization. While our $v = 0$ theory dictates that the components of \mathbf{P} must be confined to exactly zero, all integers, or even integers depending on the phase, the finite-temperature MC data in Fig. 2(c) reveal continuous deviations from these quantized values.[52] Furthermore, Fig. 2(d) shows that this loss of quantization is directly accompanied by a finite thermal monopole density. This fractional leakage of the macroscopic winding numbers mirrors our theoretical conclusion: the thermal excitation of monopoles blurs the topological distinctions between the macroscopic phases.

Conclusion and Outlook.— In conclusion, we have presented a theoretical framework that describes the thermodynamic and topological nature of the $S = 1$ pyrochlore spin ice of Blume-Capel type. By mapping the monopole-free spin configurations onto standard statistical mechanics models on the dual diamond lattice, we clarified the microscopic origins of the 3D XY and 3D Ising universality classes, and provided theoretical estimates for the phase boundaries of the U(1) Coulomb and spin nematic phases. The macroscopic flux vector serves as a topological invariant, distinguishing the phases through parity constraints on the defect strings.

Crucially, our study resolves the finite-temperature fate of these macroscopic phases. We demonstrated that the thermal excitation of monopoles alters the macroscopic topology. By acting as a symmetry-breaking field in the continuous XY wave picture, and simultaneously as a string-severing perturbation in the discrete loop-gas particle picture, thermal monopoles round the phase transitions into continuous crossovers. This scenario is supported by the absence of a macroscopic thermodynamic divergence and the fractional leakage of the quantized flux in our MC simulations.

Looking forward, our formulations provide a foundation for exploring quantum $S = 1$ spin ice [53–55]. Incorporating transverse quantum spin fluctuations could suppress thermal monopoles and endow the defect loops with quantum dynamics. Furthermore, treating the $S = 1$ spins fully quantum mechanically inherently introduces on-site quadrupolar degrees of freedom alongside the dipolar ones. The interplay between these multipolar fluctuations and the emergent gauge fields is expected to

lead to even richer exotic phenomena, opening a promising avenue for stabilizing novel quantum spin liquids or supersolid phases at zero temperature. More broadly, our framework offers a conceptual paradigm applicable to a wider class of frustrated systems. Indeed, the interplay between ice-rule constraints, emergent gauge fields, and explicit symmetry-breaking perturbations is increasingly recognized as a unifying principle across diverse physical platforms, ranging from hydrogen-bonded ferroelectrics [33] to phononic degrees of freedom in band insulators [34]. Building on this broad conceptual link, along with the established gauge-theoretic understanding of proton disorder in ambient water ice [32], our conclusion that thermal monopoles round topological phase transitions into continuous crossovers resolves a thermodynamic paradox in high-pressure water ice [56]. By mapping the hydrogen-bond network onto the present $S = 1$ spin model, the monopole screening mechanism dictates that the structural transformation between the dynamically disordered molecular ice-VII and the symmetric non-molecular ice-X lacks a thermodynamic singularity, proving that these two phases are adiabatically continuous. This highlights a universal interplay between emergent gauge theories, geometric string topologies, and macroscopic phase behaviors across diverse fields ranging from frustrated magnetism to dense molecular networks.

We thank Naoto Nagaosa, Tibor Rakovszky, and Inti Sodemann for useful discussions. The work of S.W. is supported by JST SPRING, Grant No. JPMJSP2108. The work of Y.M. is supported by JSPS KAKENHI Grant No. JP25H01247. The work of H.W. is supported by JSPS KAKENHI Grant No. JP24K00541. The work of H.W. was conducted in part during the program “Generalised symmetries and anomalies in quantum phases of matter 2026” (code: ICTS/GSYQM2026/01).

* watanabe-sena397@g.ecc.u-tokyo.ac.jp

† motome@ap.t.u-tokyo.ac.jp

‡ hwatanabe@ust.hk

- [1] L. Balents, Spin liquids in frustrated magnets, *Nature* **464**, 199 (2010).
- [2] L. Savary and L. Balents, Quantum spin liquids: a review, *Rep. Prog. Phys.* **80**, 016502 (2017).
- [3] J. Knolle and R. Moessner, A field guide to spin liquids, *Annu. Rev. Condens. Matter Phys.* **10**, 451 (2019).
- [4] C. Broholm, R. J. Cava, S. A. Kivelson, D. G. Nocera, M. R. Norman, and T. Senthil, Quantum spin liquids, *Science* **367**, eaay0668 (2020).
- [5] M. J. Harris, S. T. Bramwell, D. F. McMorrow, T. Zeiske, and K. W. Godfrey, Geometrical frustration in the ferromagnetic pyrochlore $\text{Ho}_2\text{Ti}_2\text{O}_7$, *Phys. Rev. Lett.* **79**, 2554 (1997).
- [6] A. P. Ramirez, A. Hayashi, R. J. Cava, R. Siddharthan, and B. S. Shastry, Zero-point entropy in ‘spin ice’, *Nature* **399**, 333 (1999).

- [7] S. T. Bramwell and M. J. P. Gingras, Spin ice state in frustrated magnetic pyrochlore materials, *Science* **294**, 1495 (2001).
- [8] M. J. P. Gingras and P. A. McClarty, Quantum spin ice: a search for gapless quantum spin liquids in pyrochlore magnets, *Rep. Prog. Phys.* **77**, 056501 (2014).
- [9] M. Hermele, M. P. A. Fisher, and L. Balents, Pyrochlore photons: The $U(1)$ spin liquid in a $S = 1/2$ three-dimensional frustrated magnet, *Phys. Rev. B* **69**, 064404 (2004).
- [10] S. V. Isakov, K. Gregor, R. Moessner, and S. L. Sondhi, Dipolar spin correlations in classical pyrochlore magnets, *Phys. Rev. Lett.* **93**, 167204 (2004).
- [11] C. L. Henley, Power-law spin correlations in pyrochlore antiferromagnets, *Phys. Rev. B* **71**, 014424 (2005).
- [12] D. A. Huse, W. Krauth, R. Moessner, and S. L. Sondhi, Coulomb and liquid dimer models in three dimensions, *Phys. Rev. Lett.* **91**, 167004 (2003).
- [13] R. Moessner and S. L. Sondhi, Three-dimensional resonating-valence-bond liquids and their excitations, *Phys. Rev. B* **68**, 184512 (2003).
- [14] T. Fennell, P. P. Deen, A. R. Wildes, K. Schmalzl, D. Prabhakaran, A. T. Boothroyd, R. J. Aldus, D. F. McMorrow, and S. T. Bramwell, Magnetic coulomb phase in the spin ice $\text{Ho}_2\text{Ti}_2\text{O}_7$, *Science* **326**, 415 (2009).
- [15] D. J. P. Morris, D. A. Tennant, S. A. Grigera, B. Klemke, C. Castelnovo, R. Moessner, C. Czarnik, M. Meissner, K. C. Rule, J.-U. Hoffmann, K. Kiefer, S. Gerischer, D. Slobinsky, and R. S. Perry, Dirac strings and magnetic monopoles in the spin ice $\text{Dy}_2\text{Ti}_2\text{O}_7$, *Science* **326**, 411 (2009).
- [16] C. Castelnovo, R. Moessner, and S. L. Sondhi, Magnetic monopoles in spin ice, *Nature* **451**, 42 (2008).
- [17] L. D. C. Jaubert and P. C. W. Holdsworth, Signature of magnetic monopole and dirac string dynamics in spin ice, *Nat. Phys.* **5**, 258 (2009).
- [18] I. A. Ryzhkin, Magnetic relaxation in rare-earth oxide pyrochlores, *J. Exp. Theor. Phys.* **101**, 481 (2005).
- [19] C. Castelnovo, R. Moessner, and S. L. Sondhi, Debye-Hückel theory for spin ice at low temperature, *Phys. Rev. B* **84**, 144435 (2011).
- [20] M. E. Brooks-Bartlett, S. T. Banks, L. D. C. Jaubert, A. Harman-Clarke, and P. C. W. Holdsworth, Magnetic-moment fragmentation and monopole crystallization, *Phys. Rev. X* **4**, 011007 (2014).
- [21] S. Petit, E. Lhotel, S. Guitteny, O. Florea, J. Robert, P. Bonville, I. Mirebeau, J. Ollivier, H. Mutka, E. Ressouche, C. Decorse, M. Ciomaga Hatnean, and G. Balakrishnan, Observation of magnetic fragmentation in spin ice, *Nat. Phys.* **12**, 746 (2016).
- [22] J. Rehn, A. Sen, and R. Moessner, Fractionalized \mathbb{Z}_2 classical heisenberg spin liquids, *Phys. Rev. Lett.* **118**, 047201 (2017).
- [23] N. Shannon, K. Penc, and Y. Motome, Nematic, vector-multipole, and plateau-liquid states in the classical $o(3)$ pyrochlore antiferromagnet with biquadratic interactions in applied magnetic field, *Phys. Rev. B* **81**, 184409 (2010).
- [24] Y. Wan and M. J. P. Gingras, Color ice states, weathervane modes, and order by disorder in the bilinear-biquadratic pyrochlore heisenberg antiferromagnet, *Phys. Rev. B* **94**, 174417 (2016).
- [25] J. Pandey and K. Damle, $S = 1$ pyrochlore magnets with competing anisotropies: A tale of two coulomb phases, \mathbb{Z}_2 flux confinement and XY -like transitions (2025), arXiv:2512.11623 [cond-mat.str-el].
- [26] S. Kundu and K. Damle, Flux fractionalization transition in anisotropic $S = 1$ antiferromagnets and dimer-loop models, *Phys. Rev. X* **15**, 011018 (2025).
- [27] S. Kundu and K. Damle, Flux confinement-deconfinement transition of dimer-loop models on three-dimensional bipartite lattices (2025), arXiv:2510.11607.
- [28] E. Fradkin and S. H. Shenker, Phase diagrams of lattice gauge theories with higgs fields, *Phys. Rev. D* **19**, 3682 (1979).
- [29] J. B. Kogut, An introduction to lattice gauge theory and spin systems, *Rev. Mod. Phys.* **51**, 659 (1979).
- [30] T. Senthil and M. P. A. Fisher, \mathbb{Z}_2 gauge theory of electron fractionalization in strongly correlated systems, *Phys. Rev. B* **62**, 7850 (2000).
- [31] A. Kitaev, Anyons in an exactly solved model and beyond, *Ann. Phys.* **321**, 2 (2006).
- [32] O. Benton, O. Sikora, and N. Shannon, Classical and quantum theories of proton disorder in hexagonal water ice, *Phys. Rev. B* **93**, 125143 (2016).
- [33] C.-H. Chern and N. Nagaosa, Gauge field and the confinement-deconfinement transition in hydrogen-bonded ferroelectrics, *Phys. Rev. Lett.* **112**, 247602 (2014).
- [34] Z. Han and S. A. Kivelson, Emergent gauge fields in band insulators, *Proc. Natl. Acad. Sci. U.S.A.* **122**, e2421778122 (2025).
- [35] F. J. Wegner, Duality in generalized ising models and phase transitions without local order parameters, *J. Math. Phys.* **12**, 2259 (1971).
- [36] M. Blume, Theory of the first-order magnetic phase change in UO_2 , *Phys. Rev.* **141**, 517 (1966).
- [37] H. Capel, On the possibility of first-order phase transitions in ising systems of triplet ions with zero-field splitting, *Physica* **32**, 966 (1966).
- [38] J. V. José, L. P. Kadanoff, S. Kirkpatrick, and D. R. Nelson, Renormalization, vortices, and symmetry-breaking perturbations in the two-dimensional planar model, *Phys. Rev. B* **16**, 1217 (1977).
- [39] R. Savit, Duality in field theory and statistical systems, *Rev. Mod. Phys.* **52**, 453 (1980).
- [40] K. Hattori and H. Tsunetsugu, Classical monte carlo study for antiferro quadrupole orders in a diamond lattice, *J. Phys. Soc. Jpn.* **85**, 094001 (2016).
- [41] A. W. Sandvik and R. Moessner, Correlations and confinement in nonplanar two-dimensional dimer models, *Phys. Rev. B* **73**, 144504 (2006).
- [42] L. D. C. Jaubert, M. J. Harris, T. Fennell, R. G. Melko, S. T. Bramwell, and P. C. W. Holdsworth, Topological-sector fluctuations and curie-law crossover in spin ice, *Phys. Rev. X* **3**, 011014 (2013).
- [43] A. Nahum, J. T. Chalker, P. Serna, M. Ortuño, and A. M. Somoza, 3d loop models and the CP^{n-1} sigma model, *Phys. Rev. Lett.* **107**, 110601 (2011).
- [44] Y. Deng and H. W. J. Blöte, Simultaneous analysis of several models in the three-dimensional ising universality class, *Phys. Rev. E* **68**, 036125 (2003).
- [45] J. Nasu, T. Kaji, K. Matsuura, M. Udagawa, and Y. Motome, Phase transitions to fractionalized mott insulators in an anisotropic 3d kitaev model, *Phys. Rev. B* **89**, 115125 (2014).
- [46] See Supplemental Material for detailed derivations of the duality mapping to the XY model at finite temperatures

- and the mapping to the Ising model with a magnetic field.
- [47] C. Castelnovo and C. Chamon, Topological order in a three-dimensional toric code at finite temperature, *Phys. Rev. B* **78**, 155120 (2008).
 - [48] I. Kimchi, J. G. Analytis, and A. Vishwanath, Three-dimensional quantum spin liquids in models of harmonic-honeycomb iridates and phase diagram in an infinite- d approximation, *Phys. Rev. B* **90**, 205126 (2014).
 - [49] J. Nasu, M. Udagawa, and Y. Motome, Vaporization of kitaev spin liquids, *Phys. Rev. Lett.* **113**, 197205 (2014).
 - [50] G. T. Barkema and M. E. J. Newman, Monte carlo simulation of ice models, *Phys. Rev. E* **57**, 1155 (1998).
 - [51] R. G. Melko, B. C. den Hertog, and M. J. P. Gingras, Long-range order at low temperatures in dipolar spin ice, *Phys. Rev. Lett.* **87**, 067203 (2001).
 - [52] Note that ΔP is a system-size-dependent quantity that approaches 1/4 in the completely random limit. We expect that, as the system approaches the thermodynamic limit, ΔP converges to 1/4 for all values of μ at any finite temperature.
 - [53] L. Savary and L. Balents, Coulombic quantum liquids in spin-1/2 pyrochlores, *Phys. Rev. Lett.* **108**, 037202 (2012).
 - [54] N. Shannon, O. Sikora, F. Pollmann, K. Penc, and P. Fulde, Quantum ice: A quantum monte carlo study, *Phys. Rev. Lett.* **108**, 067204 (2012).
 - [55] O. Benton, O. Sikora, and N. Shannon, Seeing the light: Experimental signatures of emergent electromagnetism in a quantum spin ice, *Phys. Rev. B* **86**, 075154 (2012).
 - [56] S. Watanabe, Y. Motome, and H. Watanabe, Continuous crossover between high-pressure ice phases VII and X driven by monopole screening (2026), unpublished preprint.

SUPPLEMENTAL MATERIAL

Dual Mapping to the XY Model at Finite Temperatures

In the main text, we introduced the duality mapping to the classical XY model in the monopole-free limit ($v = 0$). Here, we generalize this mapping to finite temperatures, where the local constraints are relaxed and thermal monopoles with local charge $Q_{\mathbf{r}} := \nabla \cdot \mathbf{S}_{\mathbf{r}} \neq 0$ are thermally excited.

To enforce this generalized local constraint, we introduce a continuous phase field $\theta_{\mathbf{r}} \in [0, 2\pi)$ at each diamond-lattice site \mathbf{r} via the Fourier integral representation of the Kronecker delta:

$$\delta_{\nabla \cdot \mathbf{S}_{\mathbf{r}}, Q_{\mathbf{r}}} = \int_0^{2\pi} \frac{d\theta_{\mathbf{r}}}{2\pi} e^{-i\theta_{\mathbf{r}} \nabla \cdot \mathbf{S}_{\mathbf{r}} + i\theta_{\mathbf{r}} Q_{\mathbf{r}}}. \quad (19)$$

By inserting this integral into the partition function Z and performing a discrete integration by parts on the lattice, $\sum_{\mathbf{r}} \theta_{\mathbf{r}} \nabla \cdot \mathbf{S}_{\mathbf{r}} = -\sum_{\ell} \nabla \theta_{\ell} S_{\ell}^z$ (where $\nabla \theta_{\ell} := \theta_{\mathbf{r}_B} - \theta_{\mathbf{r}_A}$), we find that the spin and monopole degrees of freedom decouple. The partition function thus factorizes into link-dependent and site-dependent terms:

$$\begin{aligned} Z &= \sum_{\{Q_{\mathbf{r}}\}} \sum_{\{S_{\ell}^z\}} \prod_{\mathbf{r}} \left(\int_0^{2\pi} \frac{d\theta_{\mathbf{r}}}{2\pi} e^{-i\theta_{\mathbf{r}} \nabla \cdot \mathbf{S}_{\mathbf{r}} + i\theta_{\mathbf{r}} Q_{\mathbf{r}}} \right) v^{\sum_{\mathbf{r}} Q_{\mathbf{r}}^2} w^{\sum_{\ell} (S_{\ell}^z)^2} \\ &= \int \mathcal{D}\theta \prod_{\ell} \left(\sum_{S_{\ell}^z \in \{0, \pm 1\}} e^{iS_{\ell}^z \nabla \theta_{\ell}} w^{(S_{\ell}^z)^2} \right) \prod_{\mathbf{r}} \left(\sum_{Q_{\mathbf{r}}} v^{Q_{\mathbf{r}}^2} e^{iQ_{\mathbf{r}} \theta_{\mathbf{r}}} \right) \\ &= \int \mathcal{D}\theta \prod_{\langle \mathbf{r}, \mathbf{r}' \rangle} [1 + 2w \cos(\theta_{\mathbf{r}} - \theta_{\mathbf{r}'})] \prod_{\mathbf{r}} \left[1 + 2 \sum_{Q_{\mathbf{r}} > 0} v^{Q_{\mathbf{r}}^2} \cos(Q_{\mathbf{r}} \theta_{\mathbf{r}}) \right], \end{aligned} \quad (20)$$

where $\mathcal{D}\theta := \prod_{\mathbf{r}} \frac{d\theta_{\mathbf{r}}}{2\pi}$ is the integration measure. Note that $Q_{\mathbf{r}}$ takes integer values ranging from -4 to 4 , representing the discrete divergence of four spins at a site.

In the low-temperature regime ($w \ll 1$ and $v \ll 1$), we employ the Taylor expansion $\ln(1 + X) \approx X$. Since the statistical weight scales as $v^{Q_{\mathbf{r}}^2}$, the summation is dominated by the fundamental monopole excitations ($Q_{\mathbf{r}} = \pm 1$). Neglecting higher-order terms, the partition function converges to the effective action:

$$Z \approx \int \mathcal{D}\theta \exp \left[2w \sum_{\langle \mathbf{r}, \mathbf{r}' \rangle} \cos(\theta_{\mathbf{r}} - \theta_{\mathbf{r}'}) + 2v \sum_{\mathbf{r}} \cos \theta_{\mathbf{r}} \right]. \quad (21)$$

This result confirms that the thermal monopoles manifest as a uniform external magnetic field (a sine-Gordon potential) coupled to the emergent XY phase variables.

Mapping to the Ising Model with a Magnetic Field

To investigate the effects of thermal monopoles ($v > 0$) in the large- w regime, we generalize Pauling's approximation to configurations with nonzero monopole charges and establish a term-by-term correspondence with the high-temperature expansion of the 3D Ising model in a magnetic field.

At finite temperatures, thermal monopoles geometrically act as endpoints of the defect strings. The partition function can be expressed as a sum over general graph configurations G that may contain endpoints and self-intersections:

$$Z = w^{2N} \sum_G \left(\frac{1}{w} \right)^{|G|} W_v(G), \quad (22)$$

where $W_v(G)$ is the weighted number of valid background spin configurations for a fixed graph G , defined by

$$W_v(G) := \sum_{\{Q_{\mathbf{r}}\}} \sum_{\{S_{\ell}^z\}} \left(\prod_{\mathbf{r}} \delta_{\nabla \cdot \mathbf{S}_{\mathbf{r}}, Q_{\mathbf{r}}} \right) \left(\prod_{\ell \in G} \delta_{S_{\ell}^z, 0} \right) \left(\prod_{\ell \notin G} \delta_{|S_{\ell}^z|, 1} \right) v^{\sum_{\mathbf{r}} Q_{\mathbf{r}}^2}. \quad (23)$$

Let $d_0(\mathbf{r})$ be the number of defect links (fixed to $S_\ell^z = 0$) connected to a given site \mathbf{r} . The remaining $4 - d_0(\mathbf{r})$ links can freely take ± 1 . We define the local state sum $z(d_0)$ by summing the statistical weight v^{Q^2} over all 2^{4-d_0} possible assignments:

$$z(d_0) := \sum_Q \binom{4-d_0}{\frac{4-d_0+Q}{2}} v^{Q^2}. \quad (24)$$

In the low-temperature regime ($v \ll 1$), we neglect higher-order monopole contributions (e.g., v^4). The local state sums are evaluated as:

$$\begin{aligned} d_0 = 0: & \quad Q = 0 \text{ dominates, giving } z(0) \approx \binom{4}{2} v^0 = 6. \\ d_0 = 1: & \quad Q = \pm 1, \text{ giving } z(1) \approx 2 \binom{3}{1} v = 6v. \\ d_0 = 2: & \quad Q = 0 \text{ dominates, giving } z(2) \approx \binom{2}{1} v^0 = 2. \\ d_0 = 3: & \quad Q = \pm 1, \text{ giving } z(3) \approx 2 \binom{1}{0} v = 2v. \\ d_0 = 4: & \quad Q = 0, \text{ giving } z(4) = \binom{0}{0} v^0 = 1. \end{aligned} \quad (25)$$

Under Pauling's approximation, the total weight $W_v(G)$ is estimated by multiplying the $2^{2N-|G|}$ completely free degrees of freedom by the probabilities $z(d_0)/2^{4-d_0}$ for realizing the specific charge configurations at all sites:

$$W_v(G) \approx 2^{2N-|G|} \prod_{\mathbf{r}} \frac{z(d_0(\mathbf{r}))}{2^{4-d_0(\mathbf{r})}} = 2^{|G|-2N} \prod_{\mathbf{r}} z(d_0(\mathbf{r})), \quad (26)$$

where we used the identity $\sum_{\mathbf{r}} [4 - d_0(\mathbf{r})] = 4N - 2|G|$. Let V_k denote the number of sites in graph G with degree k (i.e., $d_0(\mathbf{r}) = k$). The product over sites becomes $z(0)^{V_0} z(1)^{V_1} z(2)^{V_2} z(3)^{V_3} z(4)^{V_4}$. Factoring out the vacuum weight $W(\emptyset) \approx 2^{-2N} z(0)^N$ and using $V_0 = N - V_1 - V_2 - V_3 - V_4$, we obtain

$$\begin{aligned} W_v(G) & \approx W(\emptyset) 2^{|G|} \left(\frac{z(1)}{z(0)} \right)^{V_1} \left(\frac{z(2)}{z(0)} \right)^{V_2} \left(\frac{z(3)}{z(0)} \right)^{V_3} \left(\frac{z(4)}{z(0)} \right)^{V_4} \\ & = W(\emptyset) 2^{|G|} v^{V_1} \left(\frac{1}{3} \right)^{V_2} \left(\frac{v}{3} \right)^{V_3} \left(\frac{1}{6} \right)^{V_4}. \end{aligned} \quad (27)$$

We eliminate V_2 by exploiting the graph-theoretic identity for the sum of degrees: $V_1 + 2V_2 + 3V_3 + 4V_4 = 2|G| \implies V_2 = |G| - \frac{1}{2}V_1 - \frac{3}{2}V_3 - 2V_4$. This yields

$$\begin{aligned} W_v(G) & \approx W(\emptyset) 2^{|G|} v^{V_1} \left[\left(\frac{1}{3} \right)^{|G|} (\sqrt{3})^{V_1} (3\sqrt{3})^{V_3} 9^{V_4} \right] \left(\frac{v}{3} \right)^{V_3} \left(\frac{1}{6} \right)^{V_4} \\ & = W(\emptyset) \left(\frac{2}{3} \right)^{|G|} (\sqrt{3}v)^{V_1+V_3} \left(\frac{3}{2} \right)^{V_4}. \end{aligned} \quad (28)$$

The sum of odd-degree vertices $V_1 + V_3$ corresponds to the total number of endpoints $|\partial G|$ in the graph. Assuming a dilute gas where self-intersections (V_4) are rare, we approximate $(3/2)^{V_4} \approx 1$. The partition function then simplifies to

$$Z \approx w^{2N} W(\emptyset) \sum_G \left(\frac{2}{3w} \right)^{|G|} (\sqrt{3}v)^{|\partial G|}. \quad (29)$$

We compare this result with the high-temperature expansion of the 3D Ising model in a uniform external magnetic field h , defined as $Z_{\text{Ising}} = \sum_{\{\sigma_{\mathbf{r}}\}} \exp \left(K \sum_{\langle \mathbf{r}, \mathbf{r}' \rangle} \sigma_{\mathbf{r}} \sigma_{\mathbf{r}'} + h \sum_{\mathbf{r}} \sigma_{\mathbf{r}} \right)$. The expansion yields

$$Z_{\text{Ising}} = (\cosh K)^{2N} (\cosh h)^N 2^N \sum_G x^{|G|} y^{|\partial G|}. \quad (30)$$

This establishes a mapping between the microscopic physical parameters and the effective Ising parameters:

$$x := \tanh K = \frac{2}{3w}, \quad (31)$$

$$y := \tanh h = \sqrt{3}v. \quad (32)$$